Available online at www.sciencedirect.com
SCIENCE DIRECT®
ELSEVIER
Scripta Materialia 55 (2006) 311–314
Scripta MATERIALIA
www.actamat-journals.com

Inherent internal friction of B2 → R and R → B19′ martensitic transformations in equiatomic TiNi shape memory alloy

S.H. Chang and S.K. Wu*

Department of Materials Science and Engineering, National Taiwan University, 1 Roosevelt Rd. Sec. 4, Taipei 106, Taiwan, ROC

Received 15 March 2006; revised 19 April 2006; accepted 28 April 2006
Available online 26 May 2006

The inherent internal frictions $IF_{PT}^{B2\rightarrow R} + IF_I$ and $IF_{PT}^{R\rightarrow B19'} + IF_I$ of $Ti_{50}Ni_{50}$ alloy are studied under isothermal conditions. The $\tan\delta$ values of $IF_{PT}^{B2\rightarrow R} + IF_I$ and $IF_{PT}^{R\rightarrow B19'} + IF_I$ are both proportional to $\sigma_0/\upsilon^{1/2}$ and thus the damping mechanism of $IF_{PT}^{B2\rightarrow R} + IF_I$ and $IF_{PT}^{R\rightarrow B19'} + IF_I$ is related to the stress-assisted martensitic transformation and stress-assisted motions of twin boundary. The $\tan\delta$ value of $IF_{PT}^{R\rightarrow B19'} + IF_I$ is larger than that of $IF_{PT}^{B2\rightarrow R} + IF_I$ because of the larger transformation strain and the greater twin boundaries associated with the R → B19′ transformation.

Keywords: Shape memory alloys (SMA); Martensitic phase transformation; Internal friction; Dynamic mechanical analysis

TiNi-based alloys exhibiting a thermoelastic martensitic transformation are known as the most important shape memory alloys (SMAs) with a good shape memory effect and superelasticity [1]. It has also been reported that TiNi SMAs perform a high level of mechanical damping and are suitable for energy dissipation applications [2–9]. The high damping obtained in both R-phase and B19′ martensite of TiNi SMAs is attributed to the movement of their twin boundaries [5]. In addition, the occurrence of R-phase can significantly soften the storage modulus E_0 and thus promote the damping capacity of TiNi SMAs [10].

It has been proposed that the internal friction of a first-order phase transformation can be decomposed into three terms: IF_{Tr}, IF_{PT}, and IF_I [11–14]. The first term IF_{Tr} is a transitory internal friction which appears only at low frequency and non-zero heating/cooling rates. The second term IF_{PT} is the internal friction due to phase transformation, but it does not depend on the heating and cooling rates. The third term IF_I is the intrinsic internal friction of the austenitic or martensitic phase.

All of the aforementioned reports focus on studies involving IF_{Tr} characteristics; however, the inherent internal friction ($IF_{PT} + IF_I$) of TiNi SMAs associated with the phase transformation under isothermal conditions has not been systematically investigated. In this study, equiatomic TiNi SMA was severely cold-rolled and then annealed at 650 °C for 2 min to obtain a two-stage B2 → R → B19′ transformation during cooling. The damping capacity $\tan\delta$ values of B2 → R → B19′ martensitic transformation were measured using a dynamic mechanical analyzer (DMA) under isothermal conditions at different temperatures. The isothermal damping characteristics of B2 → R and R → B19′ transformations are discussed.

Equiatomic $Ti_{50}Ni_{50}$ alloy was prepared by conventional vacuum arc remelting. The as-melted ingot was hot-rolled at 850 °C into a 2 mm thick plate and then the plate was solution-treated at 850 °C for 2 h followed by quenching in water. Then, the plate was cold-rolled at room temperature along the hot-rolling direction and reached a final 30% thickness reduction. No annealing was conducted during cold-rolling so as to avoid the occurrence of recrystallization. Subsequently, the cold-rolled plate was cut into test specimens, sealed in an evacuated quartz tube and annealed at 650 °C for 2 min.

Transformation temperatures of cold-rolled and annealed specimens were determined by differential scanning calorimetry (DSC) using TA Q10 DSC equipment. The weight of the specimen used in DSC was about 30 mg and the heating and cooling rates were set at 10 °C/min. Specimens for DMA experiment were cut to the dimensions $40 \times 5 \times 1.26\ mm^3$ along the rolling direction to eliminate the influence of rolling texture [15]. Tan δ and storage modulus E_0 were measured by

* Corresponding author. Tel.: +886 2 2363 7846; fax: +886 2 2363 4562; e-mail: skw@ntu.edu.tw

1359-6462/$ - see front matter
doi:10.1016/j.scriptamat.2006.04.044

TA 2980 DMA equipment using various cooling rates, amplitudes and frequencies. The inherent damping characteristics of the specimens were also investigated by DMA, but tested under isothermal conditions. The detailed procedure for the isothermal DMA test was conducted as follows. The specimen was initially cooled at a constant cooling rate, starting from 150 °C, and was kept isothermally for 30 min at the set temperature. After this, the specimen was heated to 150 °C to ensure it had returned to the B2 parent phase. Then, the specimen was cooled to another temperature and kept isothermally at that temperature for 30 min, and so on. During the isothermal conditions, the set temperature was chosen to be in between +80 °C and −80 °C in which the $B2 \rightarrow R \rightarrow B19'$ two-stage martensitic transformation can be covered.

Figure 1(a) and (b) shows the DSC and DMA curves, respectively, of 30% cold-rolled $Ti_{50}Ni_{50}$ alloy annealed at 650 °C for 2 min. In Figure 1(a), there are two transformation peaks, i.e. $B2 \rightarrow R$ and $R \rightarrow B19'$, in the forward transformation and one $B19' \rightarrow B2$ transformation peak in the reverse. Figure 1(b) illustrates the $\tan\delta$ and storage modulus E_0 curves of the specimen of Figure 1(a). Only the cooling curves with $\dot{T} = 1$ °C/min, $\upsilon = 1$ Hz and amplitude of $\sigma_0 = 5$ μm are shown in Figure 1(b) for clarity. Two peaks also appear in the $\tan\delta$ curve which correspond to the $B2 \rightarrow R$ and $R \rightarrow B19'$ transformation peaks observed in the DSC curve shown in Figure 1(a). The peak temperatures measured by DSC and DMA tests show a small shift due to different cooling rates and specimen sizes. Except for the aforementioned $\tan\delta$ transformation peaks, an extra broad peak is also observed in Figure 1(b) at about −65 °C. This extra peak is known as the relaxation peak [4], but it is not observed in the DSC curve.

Figure 2 plots the $\tan\delta$ values vs. isothermal interval (0–30 min) of Figure 1 specimen under isothermal conditions. In Figure 2, $\tan\delta$ values of both the $B2 \rightarrow R$ and $R \rightarrow B19'$ transformations decrease with increasing isothermal intervals and reach a steady value after 10–15 min. From the $B2 \rightarrow R$ and $R \rightarrow B19'$ peaks, the decayed $\tan\delta$ values during isothermal conditions represent the aforementioned transitory internal friction IF_{Tr} which is associated with the magnitude of $\dot{T}$, and the steady $\tan\delta$ values after 15 min of isothermal conditions are the inherent internal friction $IF_{PT} + IF_{I}$ during phase transformation which is independent of $\dot{T}$. At

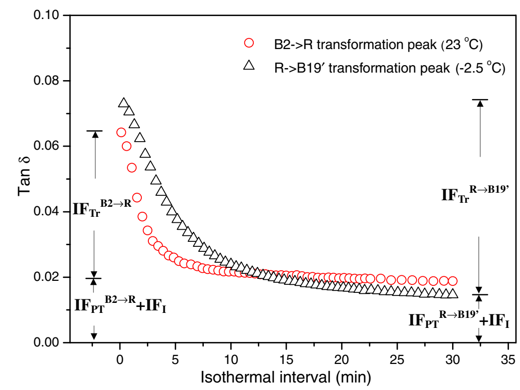

Figure 2. $\tan\delta$ values vs. isothermal interval for Figure 1 specimen measured at $\upsilon = 1$ Hz, $\sigma_0 = 5$ μm and isothermally at 23 °C ($B2 \rightarrow R$ martensitic transformation) and −2.5 °C ($R \rightarrow B19'$ martensitic transformation).

the same time, the IF_{Tr} of the $B2 \rightarrow R$ transformation under isothermal conditions, say $IF_{Tr}^{B2\rightarrow R}$, will collapse much faster than the $IF_{Tr}^{R\rightarrow B19'}$ of the $R \rightarrow B19'$ transformation.

In order to investigate the inherent internal friction for the $B2 \rightarrow R$ and $R \rightarrow B19'$ transformations, DMA $\tan\delta$ tests under 30 min of isothermal conditions were conducted at different temperatures and the results are exhibited in Figure 3. The $\tan\delta$ curve of Figure 1(b)

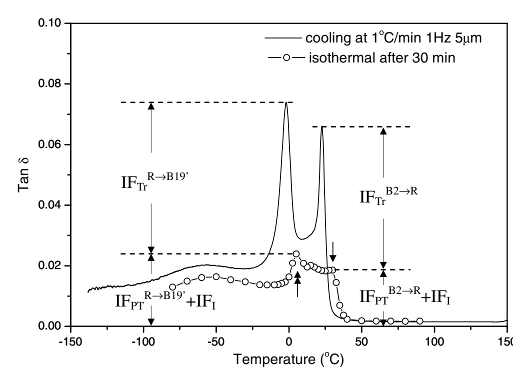

Figure 3. $\tan\delta$ values vs. temperature for Figure 1 specimen measured at $\upsilon = 1$ Hz, $\sigma_0 = 5$ μm. The solid curve is measured at $\dot{T} = 1$ °C/min and the empty circle curve is the data of the specimen kept isothermally for 30 min.

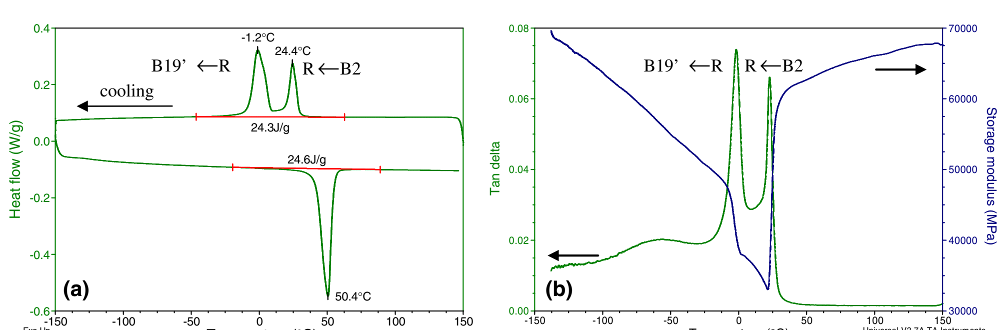

Figure 1. (a) DSC curves measured at $\dot{T} = 10$ °C/min, (b) $\tan\delta$ and storage modulus E_0 curves measured at $\dot{T} = 1$ °C/min, $\upsilon = 1$ Hz and $\sigma_0 = 5$ μm for 30% cold-rolled $Ti_{50}Ni_{50}$ alloy annealed at 650 °C for 2 min.

(measured at $\dot{T} = 1\ ^\circ\mathrm{C/min}$) is also plotted in Figure 3 for the purposes of comparison. When the isothermal temperature is set at about 30 °C, as indicated by the arrow, an inherent $\tan\delta$ peak corresponding to the B2 → R transformation, say $IF_{PT}^{B2\to R} + IF_I$, appears with a $\tan\delta$ value of 0.018. The temperature shift between the $IF_{PT}^{B2\to R} + IF_I$ peak of Figure 3 and the B2 → R transformation peak of Figure 1(b) is due to the cooling rate effect. When the isothermal temperature is set at about 5 °C, as indicated by the double arrow, another inherent internal friction peak corresponding to the R → B19′ transformation, i.e. $IF_{PT}^{R\to B19'} + IF_I$, appears with a $\tan\delta$ value of 0.024.

Figure 4(a)–(c) shows the inherent $\tan\delta$ curves measured under isothermal conditions at different $\dot{T}$, υ and σ_0, respectively. As shown in Figure 4(a), all the damping behaviors during phase transformation are similar when measured at different $\dot{T}$. Figure 5(a) plots the $\tan\delta$ values of $IF_{PT}^{B2\to R} + IF_I$ and $IF_{PT}^{R\to B19'} + IF_I$ as a function of $\dot{T}$ measured in Figure 4(a). This figure shows that the magnitudes of $IF_{PT} + IF_I$ measured at different $\dot{T}$ are almost the same for the B2 → R and R → B19′ transformations. It indicates that both $IF_{PT}^{B2\to R} + IF_I$ and $IF_{PT}^{R\to B19'} + IF_I$ are independent of $\dot{T}$. Additionally, from Figure 4(b) and (c), the $\tan\delta$ values of $IF_{PT}^{B2\to R} + IF_I$ and $IF_{PT}^{R\to B19'} + IF_I$ decrease with increasing υ but increase with increasing σ_0. Figure 5(b) plots the $\tan\delta$ values of $IF_{PT}^{B2\to R} + IF_I$ and $IF_{PT}^{R\to B19'} + IF_I$ as a function of υ measured in Figure 4(b). It makes clear that the relation between $IF_{PT} + IF_I$ and υ is non-linear; however, a linear relation between $IF_{PT} + IF_I$ and $1/\upsilon^{1/2}$ for both $IF_{PT}^{B2\to R} + IF_I$ and $IF_{PT}^{R\to B19'} + IF_I$ is observed and shown in Figure 5(c). Figure 5(d) plots the $\tan\delta$ values of $IF_{PT}^{B2\to R} + IF_I$ and $IF_{PT}^{R\to B19'} + IF_I$ as a function of σ_0 measured in Figure 4(c). In Figure 5(d), the magnitudes of both $IF_{PT}^{B2\to R} + IF_I$ and $IF_{PT}^{R\to B19'} + IF_I$ are linearly proportional to σ_0. Also in Figure 5, note that the $\tan\delta$ values of $IF_{PT}^{R\to B19'} + IF_I$ are always larger than those of $IF_{PT}^{B2\to R} + IF_I$ measured at various parameters.

As shown in Figure 1(b), for cold-rolled and annealed $Ti_{50}Ni_{50}$ SMA, there are two internal friction peaks corresponding to B2 → R and R → B19′ transformations when the DMA test is conducted at constant $\dot{T}$. After the specimen is isothermal-treated (i.e. $\dot{T} = 0$) at peak temperatures of the B2 → R and R → B19′ transformations, however, the $\tan\delta$ values decrease and only $IF_{PT}^{B2\to R} + IF_I$ and $IF_{PT}^{R\to B19'} + IF_I$ linger, as shown in Figure 3. In Figure 5(a), both $IF_{PT}^{B2\to R} + IF_I$ and $IF_{PT}^{R\to B19'} + IF_I$ are independent of $\dot{T}$ and hence their damping mechanisms cannot be explained by Delorme's model [11]. As illustrated in Figure 5(c) and (d), both the

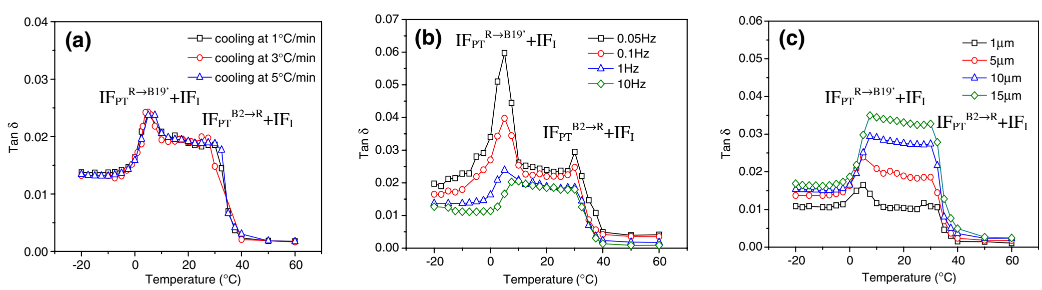

Figure 4. The inherent $\tan\delta$ curves measured under isothermal conditions at (a) $\upsilon = 1$ Hz and $\sigma_0 = 5$ μm with different $\dot{T}$, (b) at $\dot{T} = 1\ ^\circ\mathrm{C/min}$ and $\sigma_0 = 5$ μm with different υ and (c) at $\dot{T} = 1\ ^\circ\mathrm{C/min}$ and $\upsilon = 1$ Hz with different σ_0.

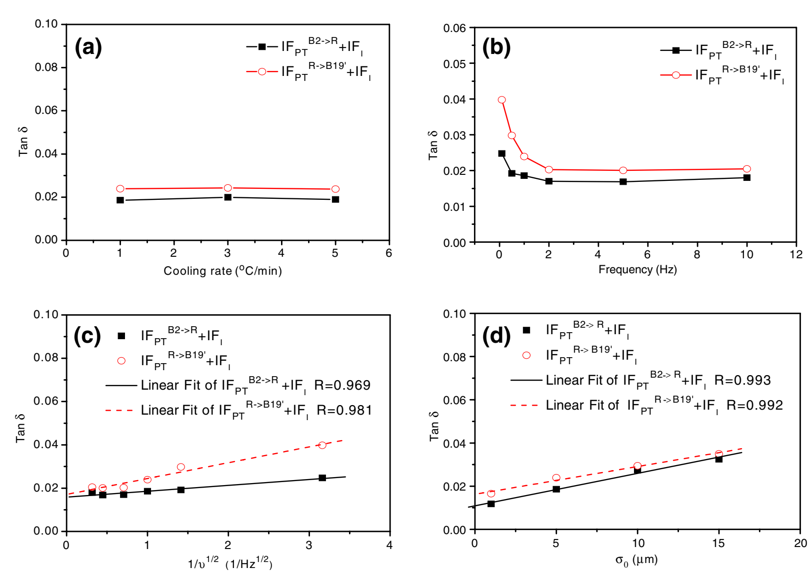

Figure 5. $\tan\delta$ values of $IF_{PT}^{B2\to R} + IF_I$ and $IF_{PT}^{R\to B19'} + IF_I$ obtained in Figure 4 as a function of (a) $\dot{T}$, (b) υ (c) $1/\upsilon^{1/2}$ and (d) σ_0.

$\tan\delta$ values of $IF_{PT}^{B2\to R} + IF_I$ and $IF_{PT}^{R\to B19'} + IF_I$ are linearly proportional to $\sigma_0/\upsilon^{1/2}$ when the applied υ and σ_0 are within 10 Hz and 15 μm, respectively. This feature is closely related to the formation of abundant twin boundaries and phase interfaces during the B2 → R → B19′ martensitic transformation. The amplitude of stress-assisted martensitic transformation can increasingly correspond with increasing σ_0 and hence lead to a higher energy dissipation of IF_{PT}. This characteristic corresponds with Dejonghe's model [12] which proposed that the $\tan\delta$ value of IF_{PT} is linearly proportional to the σ_0 measured at $\dot{T} = 0$. Besides, the $\tan\delta$ value of IF_I in R-phase and B19′ martensite which is corresponding to the stress-assisted motions of twin boundary also increases with increasing σ_0. Consequently, we conclude that $\tan\delta$ values of $IF_{PT}^{B2\to R} + IF_I$ and $IF_{PT}^{R\to B19'} + IF_I$ are linearly related to $\sigma_0/\upsilon^{1/2}$ and independent of $\dot{T}$. This indicates that the damping mechanism of $IF_{PT} + IF_I$ is mainly generated from stress-assisted martensitic transformation and stress-assisted motions of twin boundary during martensitic transformation but not from thermal-induced martensitic transformation.

Meanwhile, as illustrated in Figures 4 and 5, the $\tan\delta$ values of $IF_{PT}^{R\to B19'} + IF_I$ are always larger than those of $IF_{PT}^{B2\to R} + IF_I$ under the same conditions. This is owing to the transformation strain of R → B19′ being larger than that of B2 → R transformation [5]. Moreover, it is well known that there is an abundance of twin boundaries in the R-phase and B19′ martensite of TiNi SMAs. These twin boundaries can self-accommodate the strain which comes from the stress-induced movement of twin boundaries between the variants of R-phase or B19′ martensite. Both R-phase and transformed B19′ martensite subsist during the R → B19′ transformation, while only transformed the R-phase appears during the B2 → R transformation. Accordingly, more twin boundaries result in a greater dissipation of energy and a higher $\tan\delta$ peak during the R → B19′ transformation.

In conclusion, both $\tan\delta$ values of inherent internal friction $IF_{PT}^{B2\to R} + IF_I$ corresponding to the B2 → R transformation and $IF_{PT}^{R\to B19'} + IF_I$ corresponding to the R → B19′ transformation are linearly proportional to $\sigma_0/\upsilon^{1/2}$ but independent of $\dot{T}$. The damping mechanism of $IF_{PT}^{B2\to R} + IF_I$ and $IF_{PT}^{R\to B19'} + IF_I$ is mainly generated from the stress-assisted martensitic transformation and stress-assisted motions of twin boundary, but not from thermal-induced martensitic transformation. The $\tan\delta$ values of $IF_{PT}^{R\to B19'} + IF_I$ are always larger than those of $IF_{PT}^{B2\to R} + IF_I$ due to the larger transformation strain and the greater amount of twin boundaries associated with R → B19′ transformation.

The authors gratefully acknowledge the financial support for this research provided by the National Science Council (NSC), Taiwan, Republic of China, under Grants Nos. NSC93-2216-E002-003.

[1] C.M. Wayman, T.W. During, in: T.W. During, K.N. Melton, D. Stöckel, C.M. Wayman (Eds.), Engineering Aspects of Shape Memory Alloys, Butterworth-Heinemam, London, 1990, pp. 3–20.
[2] K. Iwasaki, R. Hasiguti, Trans. JIM 28 (1987) 363.
[3] O. Mercier, K.N. Melton, Y. De Préville, Acta Metall. 27 (1979) 1467.
[4] S.K. Wu, H.C. Lin, T.S. Chou, Acta Metall. 38 (1990) 95.
[5] H.C. Lin, S.K. Wu, M.T. Yeh, Metall. Mater. Trans. A 24 (1993) 2189.
[6] K. Sugimoto, T. Mori, K. Otsuka, K. Shimizu, Scripta Metall. 8 (1974) 1341.
[7] Y. Liu, J. Van Humbeeck, R. Stalmans, L. Delaey, J. Alloys Compd. 247 (1997) 115.
[8] B. Coluzzi, A. Biscarini, R. Campanella, L. Trotta, G. Mazzolai, A. Tuissi, F.M. Mazzolai, Acta Mater. 47 (1999) 1965.
[9] S.K. Wu, H.C. Lin, J. Alloys Compd. 72–78 (2003) 355.
[10] S.H. Chang, S.K. Wu, Key Eng. Mater. 319 (2006) 9.
[11] J.F. Delorme, R. Schmid, M. Robin, P. Gobin, J. Phys. 32 (1971) C2-101.
[12] W. Dejonghe, R. De Batist, L. Delaey, Scripta Metall. 10 (1976) 1125.
[13] J.E. Bidaux, R. Schaller, W. Benoit, J. Phys. 46 (1985) C10-601.
[14] J. Van Humbeek, J. Stoiber, L. Delaey, R. Gotthardt, Z. Metalkd. 86 (1995) 1976.
[15] S.H. Chang, S.K. Wu, Scripta Mater. 50 (2004) 937.